REPORT DOCUMENTATION PAGE

Form Approved

OMB No. 0704-0188

1. REPORT DATE *(DD-MM-YYYY)*	2. REPORT TYPE	3. DATES COVERED *(From - To)*
21-09-2015	Final	26 May 2011 to 25 May 2015

4. TITLE AND SUBTITLE

Model Development for Graphene Spintronics

5a. CONTRACT NUMBER
FA2386-11-1-4058

5b. GRANT NUMBER
Grant AOARD-114058

5c. PROGRAM ELEMENT NUMBER
61102F

6. AUTHOR(S)

Prof. P. Paul Ruden

5d. PROJECT NUMBER

5e. TASK NUMBER

5f. WORK UNIT NUMBER

7. PERFORMING ORGANIZATION NAME(S) AND ADDRESS(ES)
University of Minnesota
200 Union Street SE
Minneapolis 55455
United States

8. PERFORMING ORGANIZATION REPORT NUMBER

N/A

9. SPONSORING/MONITORING AGENCY NAME(S) AND ADDRESS(ES)

AOARD
UNIT 45002
APO AP 96338-5002

10. SPONSOR/MONITOR'S ACRONYM(S)

AFRL/AFOSR/IOA(AOARD)

11. SPONSOR/MONITOR'S REPORT NUMBER(S)
AOARD-114058

12. DISTRIBUTION/AVAILABILITY STATEMENT

Distribution A: Approved for public release. Distribution is unlimited

13. SUPPLEMENTARY NOTES

14. ABSTRACT

The goal is to develop charge and spin carrier scattering models and device models, and to explore the physics that enable and limit the operation of graphene spin valves. The models are based on the low energy linear dispersion relation of the graphene band structure near the dirac point. Scattering was evaluated in born approximation. Screening and transport were treated semi-classically.

15. SUBJECT TERMS

Graphene, Spintronics

16. SECURITY CLASSIFICATION OF:			17. LIMITATION OF ABSTRACT	18. NUMBER OF PAGES	19a. NAME OF RESPONSIBLE PERSON
a. REPORT	b. ABSTRACT	c. THIS PAGE			Seng Hong, Ph.D.
U	U	U	SAR	17	19b. TELEPHONE NUMBER *(Include area code)* +81-4 2511 2005

Standard Form 298 (Rev. 8/98)
Prescribed by ANSI Std. Z39.18

Model Development for Graphene Spintronics

Research Program
for the
Asian Office of Aerospace R &D
and the
Defense Advanced Research Projects Agency

FA2386-11-1-4058

Final Report

Period of Performance: 26 May 2011 to 25 May 2015

Dr. P.Paul Ruden, PI
(ruden@umn.edu, (612) 624-6350)

University of Minnesota, Minneapolis, MN 55455

I Introduction

The Model Development for Graphene Spintronics program began on 26 May 2011 and ended 25 May 2015. It was executed by the Department of Electrical and Computer Engineering, College of Science and Engineering, University of Minnesota, with Prof. P.Paul Ruden and Prof. Darryl L. Smith serving as PI and co-PI.

The regular period of performance for this program ended on 25 May 2014. However, as the departure of a key student in 2013 caused significant delays in executing the planned research, no-cost extensions of the program were requested and granted by the cognizant office, and the program ran through 25 May 2015.

Graphene is a promising material for electronic and spintronic applications due to its high carrier mobility and low intrinsic spin-orbit interaction. However, extrinsic effects may easily dominate the carrier dynamics. The principal effort of the program focused on theoretical work that can raise significantly the level of understanding of spin transport phenomena in graphene device structures. Of particular interest were structures that are under active exploration for the fabrication of spin valves.

II Preliminary investigation

The initial effort focused on a careful examination of likely candidate mechanisms for spin relaxation of electrons or holes in graphene on insulator (specifically silicon dioxide) structures. This involved discussions with several researchers at Los Alamos National Laboratory and elsewhere. As a result of these interactions it was decided to explore two mechanisms in detail.

The first mechanism under investigation was spin relaxation associated with the electric field of a charged impurity in the SiO_2 beneath the graphene layer.

A charged impurity in the SiO_2 gives rise to an electric field in its vicinity with a non-vanishing component perpendicular to the graphene layer. The graphene may contain non-equilibrium charge carriers (electrons or holes) induced by an applied voltage between the graphene and the gate beneath the SiO_2 layer. Evidently, the charge carriers in the graphene screen the Coulomb field associated with the impurity, however, a non-zero electric field in the graphene layer remains. This field has a component perpendicular to the plane of the graphene in the region close to the impurity. A perpendicular field breaks the reflection symmetry of the unperturbed graphene (point group D_{6h}) and gives rise to a Rashba spin-orbit coupling mechanism. (The perpendicular field near the impurity is an addition to the uniform field due to the gate, which also contributes to the Rashba-type spin-orbit coupling).

The physical mechanism under exploration was scattering due to the spatially modulated spin-orbit interaction. This type of scattering is rather unique, inasmuch as it requires a spatially varying field due to a charged center (impurity) not located within the plane of

the graphene. It also is quite different from the usual case of Dyakonov-Perel spin relaxation due to scattering.

The second spin relaxation mechanism under exploration is similar in origin to the first and also is primarily relevant for device structures. Here too, a spatially varying electric field perpendicular to the graphene layer induces a local Rashba-type spin-orbit interaction. In contrast to the example above, this effect occurs along the edge of a graphene layer, where fringe fields exist. A spin-flip scattering process of interest can occur if a charge carrier is specularly reflected at the edge of the graphene layer.

III Scattering calculations

The scattering mechanisms investigated during this phase of the program are associated with non-magnetic, charged impurities in the substrate (e.g. SiO_2) beneath the graphene layer. Such impurities cause an electric field that extends through the graphene and has a non-vanishing perpendicular component. Consequently, the impurity, in addition to the conventional elastic, spin-conserving scattering can give rise to spin-flip processes. The latter is a consequence of a spatially varying Rashba spin-orbit interaction caused by the electric field of the impurity in the substrate.

We consider a planar n-type graphene layer on a SiO_2 insulator that contains charged impurities at a distance z_0 from the graphene. Such impurities give rise to a Coulomb potential that is screened by the mobile charge carriers in the graphene. Since the charge centers are not located in the graphene plane, they also cause a spatially varying electric field perpendicular to the latter, and hence a spatially varying Rashba spin-orbit interaction. To be specific, we assume a positive impurity charge and a non-zero mobile equilibrium electron density in the graphene far from the impurity.

We calculate the screened potential in a non-linear Thomas Fermi approximation taking the limit of zero temperature. The screening is nonlinear because the density of states at the Fermi energy varies considerably in the vicinity of the impurity. Representative results are shown in fig. 1 for three different electron densities corresponding to Fermi energies $E_f \sim 10meV, 50meV$ and $100meV$.

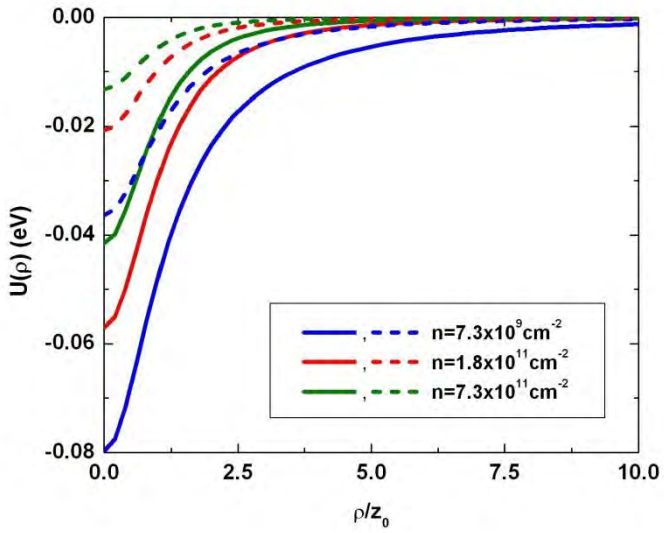

Figure 1: $U(\rho)$ as a function of ρ for several different bulk electron densities. Distances of $z_0 = 5nm$ (dashed lines) and $2.5nm$ (solid lines) are assumed.

We assume that the graphene layer is doped and electric fields far from the impurity are negligible. Hence, the electronic states are spin eigenstates. The impact of the impurity on transport is calculated in lowest order Born approximation. At this level of approximation, the two mechanisms referred to above act independently, although they are associated with the same impurity. The (lineal) differential scattering cross-section for potential scattering is calculated as,

$$\frac{d\sigma_p}{d\theta} = \frac{4}{\hbar^2 v_f{}^2}\left(\frac{k}{8\pi}\right)|U(q)|^2 cos^2\left(\frac{\theta}{2}\right)$$

Here $q = 2k\sin(\theta/2)$, and θ is the scattering angle.

We also calculate the differential cross-section for spin scattering due to the Rashba term ($R(\rho) = \alpha_R E(\rho)$, with α_R a constant related to the graphene electronic structure, and $E(\rho)$ is the perpendicular field component) as,

$$\frac{d\sigma_R}{d\theta} = \frac{1}{4\hbar^2 v_f{}^2}\left(\frac{k}{8\pi}\right)|R(q)|^2$$

III.1 Potential scattering

Results for the potential scattering cross-section as a function of the scattering angle are displayed in fig. 2 for three different electron energies, and $n = 7.3 \times 10^9 cm^{-2}$, $1.8 \times 10^{11} cm^{-2}$ and $7.3 \times 10^{11} cm^{-2}$. Evidently, back scattering is suppressed.

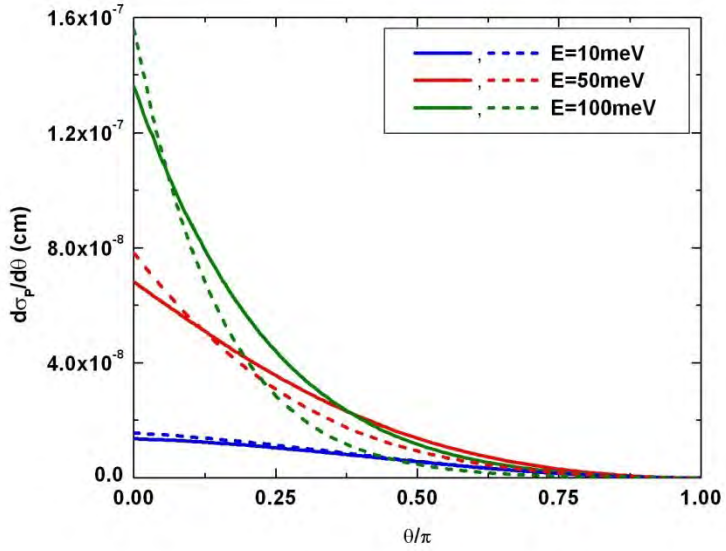

Figure 2: Differential scattering cross-section for potential scattering as a function of θ for several different electron energies, $z_0 = 5nm$ (dashed lines) and $2.5nm$ (solid lines).

III.2 Spin scattering

Results for the differential cross-section associated with the Rashba interaction due to the impurity field are plotted as a function of the scattering angle in fig. 3, again for three different electron energies corresponding to the Fermi energies for $n = 7.3 \times 10^9 cm^{-2}$, $1.8 \times 10^{11} cm^{-2}$ and $7.3 \times 10^{11} cm^{-2}$.

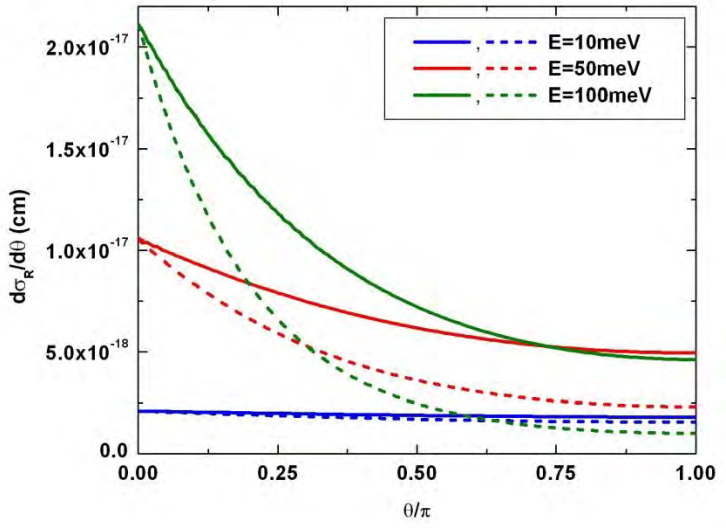

Figure 3: Differential scattering cross-section for spin scattering as a function of θ for several different electron energies, $z_0 = 5nm$ (dashed lines) and $2.5nm$ (solid lines).

Lastly, we integrate over the scattering angle to obtain the total spin-flip scattering cross-section. The results as a function of electron energy for the same parameters as above are shown in fig 4. As interest focuses primarily on electrons near the Fermi energy, the energy scale is normalized.

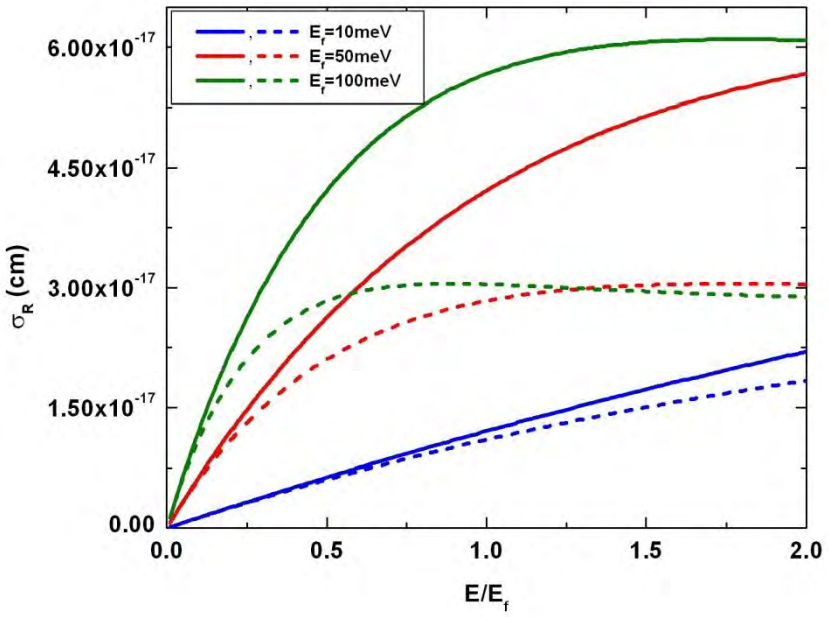

Figure 4: Total spin-scattering cross-section as a function of electron energy, $z_0 = 5nm$ (dashed lines) and $2.5nm$ (solid lines).

III.3 Momentum and spin relaxation

Both scattering mechanism addressed here can contribute to momentum relaxation. We calculate total momentum scattering cross sections by multiplying the differential cross sections above by $(1 - \cos(\theta))$ and integrating over θ. Momentum relaxation times may then be estimated for assumed densities of impurities (and distances z_0). Taking the impurity density to be $10^{11} cm^{-2}$ and $z_0 = 2.5nm$, we obtain for electrons at the Fermi energy ($E_f = 50meV$) $\tau_{m,p} \approx 2ps$ and $\tau_{m,R} \approx 3ms$. Clearly, the momentum relaxation induced by the Rashba interaction (although back-scattering is not suppressed) is quite small in comparison to the potential effect.

Spin relaxation, however, is solely associated with the Rashba term. By calculating the total integrated scattering cross-section as in fig. 5, one may estimate the spin relaxation time (for the same parameters as in the preceding discussion) to be $\tau_s \approx 2.4ms$. The early results obtained from these calculations were reported as: "Electron spin flip scattering in graphene due to substrate impurities", A. Goswami, Y. Liu, F. Liu, P.P. Ruden and D.L. Smith (2013), MRS Proceedings, 1505, mrsf12-1505-w10-12.

Further work on ionized impurity scattering conducted as part of this program aimed at a quantitative evaluation of the mechanism including the spin-orbit coupling Rashba effect throughout the graphene layer. This work led to many additional insights and was reported in detail as: "Scattering in graphene associated with charged out-of-plane impurities", Y. Liu, A. Goswami, F. Liu, D.L. Smith, and P.P. Ruden, J. Appl. Phys. 116, 234301 (2014).

III.4 Edge scattering

In graphene, the small atomic number of carbon leads to a relatively weak intrinsic spin-orbit interaction. Hence, the extrinsic spin-orbit interaction controlled by an external electric field tends to be dominant. At low temperatures carrier transport in graphene is ballistic with a mean free paths on the micron scale. These features make it possible to control the spin states by employing a field-effect-transistor-like structure. In this type of device, the edges of a graphene sheet are of interest because edge-scattering events may lead to a different spin behavior compared to the internal part. The problem is further complicated by the non-uniformity of the electrostatic field and potential near the edge. In order to understand this scenario, we explored electron spin dynamics near the edge of a graphene layer.

The Rashba spin-orbit interaction strength, Δ, is proportional to the electric field component normal to the graphene plane. The external electric field perpendicular to the graphene plane breaks the symmetry of the system and the spin states are no longer degenerate. The total graphene Hamiltonian including spin-orbit coupling can be written as:

$$H = -i\hbar v_F \vec{\sigma} \cdot \nabla + \frac{\Delta}{2}\left(\vec{\sigma} \times \vec{s}\right)_z$$

where $\vec{s}$ is the true spin of an electron, and the z direction is normal to the graphene plane. The Hamiltonian is a 4×4 matrix, which couples the pseudospin, $\vec{\sigma}$, and the true spin, $\vec{s}$.

In order to incorporate the non-uniform electric field and potential in the spin calculation, we apply a multi-step approximation. As the potential and field only depend on the direction perpendicular to the edge, y, the system is divided into a series of optimized steps along y. Within each step, the electric field and potential are approximated by an optimized constant. Therefore, the Hamiltonian for each step can be solved separately and, by matching the wavefunctions at all the step boundaries, the final outgoing spin state can be calculated. As the number of steps in the calculation increases, the results gradually approach the exact value.

Representative results are shown in fig. 5. The distance between the initial location of the electron and the graphene edge is taken to be $L = 2\mu m$ (within the mean free path at low temperature). The probabilities of the spin up state at $y = L$ are calculated as a function of the incident angle. The solid line neglects the edge effect, the dashed line

includes the position-dependent electric field but not the potential, and the dash-dotted line includes both the edge-induced field and potential. The results show that the $\theta = 90^o$ case is unaffected by the edge effect, due to the time-reversed symmetry. For $\theta < 90^o$, by including the non-uniform electric field, the same spin state moves slightly to smaller angles. The decrease of the electric field near the edge leads to a decrease of the average Rashba interaction, and the difference between the two chiral wave vectors, $k_- - k_+$, also decreases, which is proportional to Δ for $\Delta << E$. In order to maintain the same phase shift $(k_- - k_+) \cdot L_p$, the propagation distance $L_p = 2L / \sin\theta$ has to increase, therefore a smaller incident angle θ is preferred. Including the effect of the electrostatic potential, the energy E is equal to the Fermi energy plus the potential. The increase of E also leads to a decrease of $|k_- - k_+|$, as the derivative $\frac{\partial}{\partial E}|k_- - k_+| \approx -\frac{1}{4\hbar v_F}\frac{\Delta^3}{E^3}$ is negative ($\Delta << E$). Therefore the same spin behavior also shifts to a smaller angle θ. The induced electrostatic potential has a more significant effect on the spin states, because it changes the total energy E. In order to maintain the y component of $|k_- - k_+|$ for the same spin probability, k_x has to increase with E, therefore the angle is shifted significantly. On the other hand, the induced electric field shifts the Rashba interaction, which is smaller than E by orders of magnitude. The effect of the induced potential is greater for smaller incident angles because for small angles the electrons spend more time propagating near the edge.

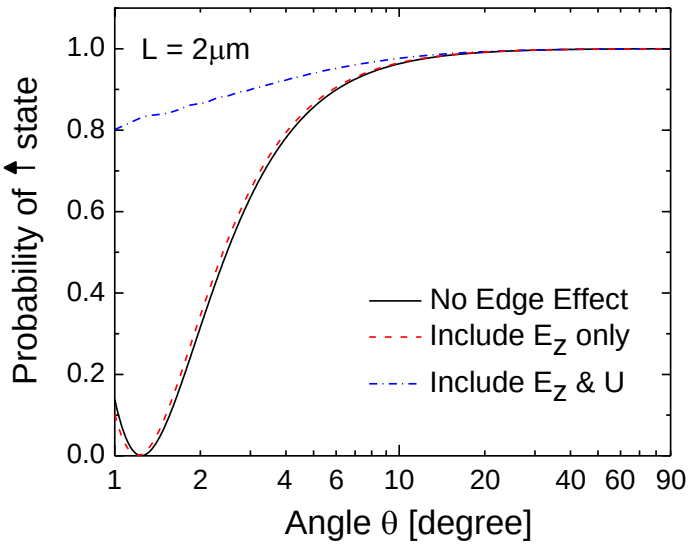

Figure 5. Probability of spin up for the outgoing state in the example device. The probability is calculated at the same distance L from the edge as the initial state. The solid line does not include the edge electrostatic effect. The dashed line includes the edge-induced electric field, but not the induced potential. The dash-dotted line includes both the edge-induced field and potential.

The key calculations of this work were described in detail as: “Rashba-induced spin scattering at graphene edges”, F. Liu,.Y. Liu, J. Hu, D.L. Smith, and P.P. Ruden, J. Appl. Phys. 114, 093708 (2013).

IV Graphene spintronic device model

In the final phase of the program we developed a device model for graphene-based spin valves that properly describes the electronic and spintronic properties, including electrostatics, charge and spin injection, transport, spin relaxation, spin-current profiles, bias-dependent magnetoresistance, etc.

A schematic cross-section of a typical graphene spin valve is shown in fig. 6. A “nonlocal” four terminal structure has been widely employed for enhanced spin injection.

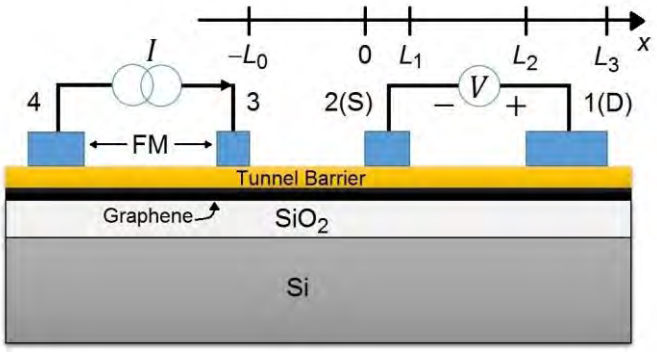

Figure 6. Schematic cross-section of a typical nonlocal graphene-based spin valve.

The four contacts 1, 2, 3, and 4 are all made of FM metals. Below the contacts is a tunnel barrier layer (on the order of 1 nm) composed of an insulating material such as Al_2O_3, to enable efficient spin injection. The graphene layer is beneath the tunnel barrier, followed by SiO_2 (on the order of 10^2 nm) and Si at the bottom providing gate control. A “current source” is applied between contacts 3 and 4, injecting and extracting both charge and spin carriers into the graphene layer. The charge current flows in one direction (3 to 4) while the spin current may flow in both directions (3 to 4, and 3 to 2). Spin detection is realized by measuring the resistance difference (called the magnetoresistance, MR) between terminals 1 and 2 in parallel (P) and antiparallel (AP) configurations.

In the following, we first discuss the simple “local” structure, which involves only two contacts, 1 and 2, and the region between them ($0 \le x \le L_3$ in fig. 6). The “local” structure is similar to a graphene field-effect transistor, except for the existence of a tunnel barrier between the graphene channel and the charge injection/collection contacts. It is convenient to use conventional transistor terminology by defining contact 2 as the “source” (S) and contact 1 as the “drain” (D). For simplicity we assume that the same definition holds for both electron and hole conduction regimes. The Si contact at the bottom constitutes the “gate” (G). After a discussion of the “local” device, we introduce

the "nonlocal" device, and discuss the bias-dependent MR for both devices in the following sections.

Because of the low density of states in graphene, a quantum capacitance effect needs to be considered. It is important to clarify three concepts in graphene: the electrostatic (Galvani) potential, *ES*, the electrochemical potential, *EC*, and the (quasi-) Fermi energy E_F. The electrostatic potential in graphene is defined as the energy per electron at the Dirac point. The electrochemical potential in graphene is defined as the energy per electron at the Fermi level. Under bias, it may be above or below the Dirac point, and it may be spin-dependent. Here we define the (quasi-) Fermi level as the difference between *EC* and *ES*, i.e., $E_F = EC - ES$. For S, D, and G contacts, we assumed infinite densities of states and $EC = ES$. The voltage (*EC* per unit charge) difference between D and S is V_{DS}. The voltage difference between G and S (D) is V_{GS} (V_{GD}). When V_{GS} is positive (negative), the Fermi level in graphene beneath the contact S is biased above (below) the Dirac point and locally the channel is in the electron (hole) conduction regime.

Because of the low density of states, the graphene layer may not completely screen the electric field induced by the charge at the gate. We introduce a screening efficiency α. For example, in the electron conduction regime, α is defined as:

$$\alpha = \frac{en}{C_S\left(V_G - V_{gph}\right)}.$$

Here, *e* is the electron charge, *n* is the electron density in graphene, C_S is the capacitance of the SiO_2 dielectric per unit area, V_G is the electrochemical or electrostatic potential at the gate, and V_{gph} is the electrostatic potential in graphene.

Under the contacts, when there is no current injection, the *EC* in graphene is the same as that in the FM contact (i.e. $E_F = eV_{gph}$). Taking the S contact as an example, the electrostatics in the vertical direction of fig. 6 satisfies the following equation:

$$eV_{GS} = E_F\left(1 + \frac{C_T}{C_S}\right) + \frac{en}{C_S}.$$

C_T is the capacitance of the tunnel barrier per unit area. When E_F is much greater than the thermal energy, the electron density *n* can be expressed in terms of E_F:

$$n = a\left(\frac{E_F^2}{2} + \frac{(\pi kT)^2}{6}\right).$$

k is the Boltzmann constant. *T* is the temperature. $a = 2\pi^{-1}(\hbar v_F)^{-2}$, where $v_F \approx 10^6$ m/s is the Fermi velocity in graphene and $\hbar$ is the reduced Planck constant.

Combining the equations above, the screening efficiency α can be written as:

$$\alpha = \left(1 + \frac{1}{AE_F}\frac{C_T}{C_S} + \frac{(\pi kT)^2}{3E_F^2}\right)^{-1}, \quad A = \frac{ae^2}{2C_S}.$$

And the Fermi level E_F is determined through:

$$E_F = \frac{1}{A}\left(1 + \frac{C_T}{C_S}\right)\left(\left(\frac{1}{4} + \frac{AeV_{GS} - \frac{(A\pi kT)^2}{3}}{\left(1 + \frac{C_T}{C_S}\right)^2}\right)^{\frac{1}{2}} - \frac{1}{2}\right).$$

In a graphene spin valve, the thickness of the tunnel barrier is about 1 nm, while the lateral dimension of the device (in x direction) is on the order of microns. Therefore in our model, it is a good approximation to assume α to be constant within each region S ($0 < x < L_1$), D ($L_2 < x < L_3$), and the channel ($L_1 < x < L_2$). The screening efficiency α is about 0.1 for S and D regions. The channel region without a contact on top corresponds to $C_T \rightarrow 0$, resulting in $\alpha \approx 1$. At $x = L_1$ and $x = L_2$, the transition of α from ~ 0.1 to ~ 1 takes place within the length scale of a few nanometers. Compared to the lateral dimension of the device, it is reasonable to assume an abrupt transition in the model.

The conductivity of graphene at a high carrier density can be written as:

$$\sigma = \frac{e^2 v_F^2}{2} D(E_F)\tau(E_F).$$

Here $D(E_F)$ is the density of states (DOS) in graphene and $\tau(E_F)$ is the momentum relaxation time, both at the Fermi level. Assuming the device to be operating at low temperature, impurity scattering is the dominant mechanism. The conductivity is then approximately proportional to E_F^2, which is consistent with experimental observations.

When S and D are FM contacts, spin-polarized carriers are injected into the graphene channel. The parameters E_F, n, and the current J all have two components, labelled by the two spin states "up", ↑, and "down", ↓. For example, $n_\uparrow$ ($n_\downarrow$) stands for the electron density with spin up (down) and the total electron density $n = n_\uparrow + n_\downarrow$. The direction of the spin is normal to the cross-section in fig. 6. We assume low injection and electron conduction regime so that the electron densities are not far from their equilibrium values. The electron-hole recombination can be neglected in this unipolar case. In the framework of the gradual channel approximation, the spin-dependent current and carrier densities can be expressed as:

$$J_{\uparrow,\downarrow} = -\kappa E_{F\uparrow,\downarrow}^2 \frac{d}{dx}\left(E_{F\uparrow,\downarrow} - eV_{gph}\right),$$

$$n_{\uparrow,\downarrow} = \frac{1}{2} a \left(\frac{E_{F\uparrow,\downarrow}^2}{2} + \frac{(\pi kT)^2}{6} \right).$$

κ is a proportionality factor determined by the physical parameters chosen. The total charge current and spin current are defined as:

$$J = J_{\uparrow} + J_{\downarrow}, \; J_S = J_{\uparrow} - J_{\downarrow}.$$

Combining these equations, the current can be expressed as functions of $E_{F\uparrow}$ and $E_{F\downarrow}$.

A spin relaxation process, which tends to reduce the net spin of the system, can occur in graphene. Physical mechanisms involve the spin-orbit interaction in combination with spatial fluctuations due to impurities, boundaries, or phonons. For the device modeling in this work, we characterize spin relaxation by a single parameter, the spin relaxation time constant, τ_S.

We take the spin relaxation time to be 0.5 ns, in agreement with relevant experimental results. When the magnetization of the two contacts S and D is in the same direction, we define it as the "parallel" (P) case, and set the spin-dependent tunneling parameter $g_{S\uparrow} = g_{D\uparrow} = 3g_{S\downarrow} = 3g_{D\downarrow}$; when S and D have opposite magnetization, we define it as the "anti-parallel" (AP) case, and set $g_{S\uparrow} = g_{D\downarrow} = 3g_{S\downarrow} = 3g_{D\uparrow}$. Typically spin valves operate at low temperature, hence we set $T = 1$ K.

IV.1 Local structure

The calculated electrochemical potential, electrostatic potential, charge and spin current density profiles for parallel and anti-parallel cases are shown in fig. 7. The device is in the electron conduction regime. The discontinuity of the electrostatic potential at the S and D boundaries are due to different screening efficiencies with and without a metal contact on top. The total current J in graphene is constant in the channel, and decreases to zero at $x = 0$ and $x = L_3$. The slight decrease of J_S in the center of the channel is due to spin relaxation. When the contacts are polarized in parallel, the spin-dependent electrochemical potentials cross, while the spin-dependent currents do not cross; when the contacts are in anti-parallel configuration, these results are opposite.

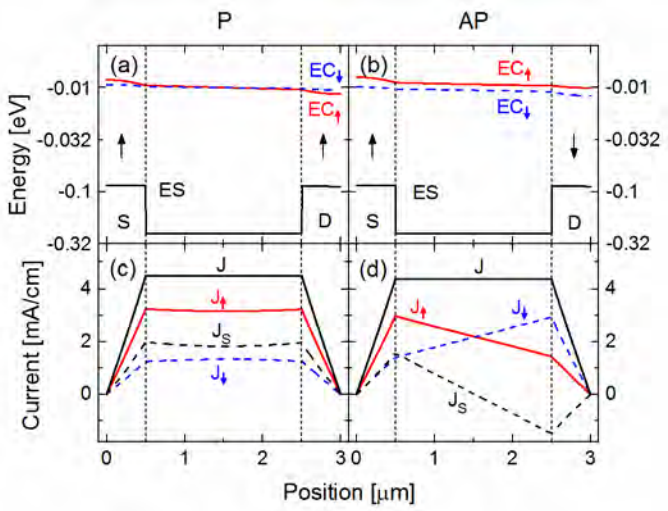

Figure 7. Electrostatic and current density profiles for a local structure. V_{DS} = 20 mV. V_{GS} = 20 V. $EC_{\uparrow}$ and $EC_{\downarrow}$ denote electrochemical potentials for spin up and spin down electrons. *ES* denotes the electrostatic potential. The current notations are defined in the text. P/AP: FM contacts with parallel/anti-parallel magnetization. The arrows denote the majority spin direction in the FM contacts. The energy is shown on a logarithmic scale.

In a "local" structure, spin and charge are injected into the device simultaneously. Hence the MR is small.

IV.2 Nonlocal structure

The introduction of a nonlocal structure is to separate the charge and spin flux, and thereby to enhance the magnetoresistive effect. As shown in fig. 6, a current source is applied between contacts 3 and 4, injecting both charge and spin into graphene. The charge current can only flow to the left while the spin current flows in both directions. The electrostatic potential on contacts 2 and 3 are set to be equal so that no charge flow occurs between them.

To understand how the nonlocal structure changes the device characteristics, in fig. 8, the spin-dependent *EC* profiles are plotted for both P and AP cases. Figs. 8 (a) and (b) show a low-bias case (V_{DS} = 2 mV), and Figs. 8 (c) and (d) show a high-bias case (V_{DS} = 10 mV). V_{GS} = 20 V is used for both cases. The black bars with "×" at the ends show the position of electrochemical potential at the S and D contacts. It is observed that most of the applied bias V_{DS} drops across the tunneling contacts. For the nonlocal device, due to spin relaxation, $EC_{\uparrow}$ - $EC_{\downarrow}$ decreases with spin flux from left to right. At low bias, the spintronic property of the device is determined by the extrinsic spin source, and the *EC*s do not cross for either P or AP cases; while at large bias, the spintronic property is dominated by intrinsic spin injection, and the *EC*s cross for the P case.

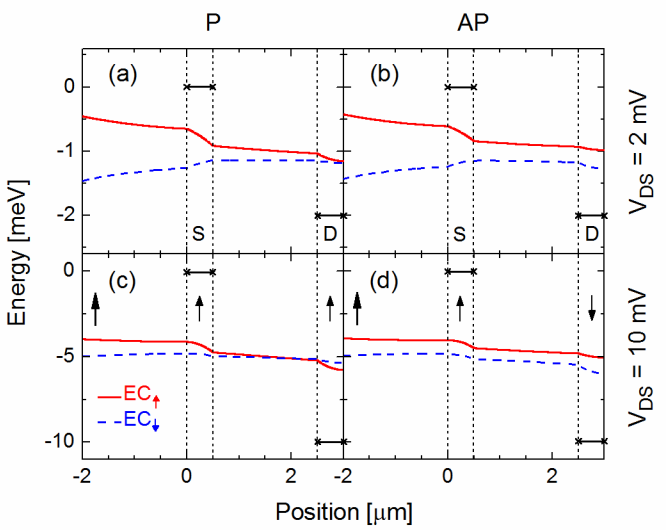

Figure 8. Spin-dependent electrochemical potential profiles for both P and AP configurations in nonlocal devices at low (V_{DS} = 2 mV) and high bias (V_{DS} = 10 mV). V_{GS} = 20 V. The black bars with "×" at the ends denote the position of electrochemical potential at the contacts. The large and small arrows indicate nonlocal spin injection and majority spin direction in the FM contacts, respectively.

The spin flux in a spin valve is detected by applying a small bias between contacts 1 and 2. In practice, one can either fix the current between 1 and 2, and measure different V_{DS} for P and AP configurations; or fix V_{DS} and measure different current for the two cases. Here, we choose the latter option, and the MR can be defined as:

$$MR = \frac{J_P}{J_{AP}} - 1$$

J_P and J_{AP} are the total current densities for P and AP configurations.

The MR and current as a function of V_{GS} for both local and nonlocal structures are plotted in fig. 9, with V_{DS} = 1 mV. For the specific set of parameters used in the calculations, MR is improved by about four times when employing a nonlocal structure. The behavior of MR as a function of V_{GS} is consistent with experimental results in the literature. For both local and nonlocal devices, MR increases with V_{GS} at small bias. For nonlocal devices, MR decreases with V_{GS} at large bias. When the magnitude of V_{GS} is small, the graphene channel is insulating; the charge and local spin transport in the channel are not very efficient. As $|V_{GS}|$ increases, the channel becomes more conducting. The voltage drop across the contact barriers increases with $|V_{GS}|$ and therefore the spin injection is more efficient. When $|V_{GS}|$ continues to increase after most of the voltage has dropped across the contact barriers, the local spin injection saturates and the decrease of the nonlocal spin injection becomes dominant.

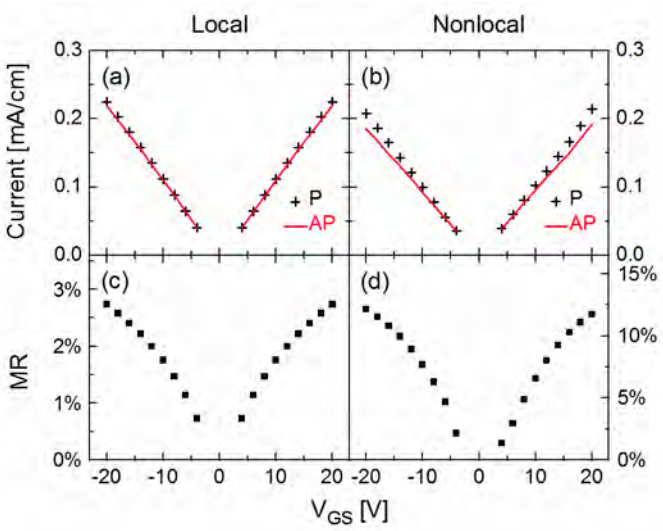

Figure 9. Current and magnetoresistance as a function of V_{GS} for both local and nonlocal structures. V_{DS} = 1 mV.

Details of the calculations as well as a more extensive presentation of the results obtained have recently been published: "Device model for graphene spin valves", F. Liu, Y. Liu, D.L. Smith, and P.P. Ruden, IEEE Trans. El. Devices 62, 3426 (2015).

V Summary

The scattering and device models developed under this program have shed much light on the physics that enable and limit the operation of local and non-local graphene spin valves. Specifically, the following problems were examined:

1) Charge carrier scattering associated with charged impurities located in the substrate that supports the graphene active layer. The mechanisms examined were the Coulomb interaction and the spatially varying Rashba spin-orbit interaction.
2) Scattering due to local electric fields at the edge of a graphene layer. Here too a novel mechanism arises due to the spatially varying Rashba interaction.
3) Local and non-local operation of graphene-based spin valves. Device model equations were developed and applied to structures that have been examined experimentally by other groups. The model results clearly indicate under which conditions significant enhancements of the magneto-resistance can be expected if the non-local operation is adopted.

The knowledge gained has been presented to the research community in great detail through one conference proceedings paper and three archival journal papers:

"Electron spin flip scattering in graphene due to substrate impurities", A. Goswami, Y. Liu, F. Liu, P.P. Ruden and D.L. Smith (2013), MRS Proceedings, 1505, mrsf12-1505-w10-12 doi:10.1557/opl.2013.246.

"Rashba-induced spin scattering at graphene edges", F. Liu,.Y. Liu, J. Hu, D.L. Smith, and P.P. Ruden, J. Appl. Phys. 114, 093708 (2013). http://dx.doi.org/10.1063/1.4820463

"Scattering in graphene associated with charged out-of-plane impurities", Y. Liu, A. Goswami, F. Liu, D.L. Smith, and P.P. Ruden, J. Appl. Phys. 116, 234301 (2014). Doi: 10.1063/1.4904193.

"Device model for graphene spin valves", F. Liu, Y. Liu, D.L. Smith, and P.P. Ruden, IEEE Trans. El. Devices 62, 3426 (2015). http://dx.doi.org/10.1109/TED.2015.2464793.

Of the students whose research was partially supported by this grant, Ms. A. Goswami graduated with an MSEE and is now employed by Intel-Micron Flash Technologies, Salt Lake City, UT. Dr. F. Liu graduated with a PhD and is now with the University of Eindhoven, Eindhoven, The Netherlands.